# Laminar Flow Past a Confined Cylinder

V.M. Ribeiro[1], P.M. Coelho[2], F.T. Pinho[2] and M.A. Alves[1]

[1]Universidade do Porto, Faculdade de Engenharia, Departamento de Engenharia Química, CEFT, Rua Dr. Roberto Frias, 4200-465 Porto, Portugal
email: vera@fe.up.pt , mmalves@fe.up.pt
[2]Universidade do Porto, Faculdade de Engenharia, Departamento de Engenharia Mecânica, CEFT, Rua Dr. Roberto Frias, 4200-465 Porto, Portugal
email: pmc@fe.up.pt , fpinho@fe.up.pt

**Abstract**

In this work we study experimentally and numerically the laminar Newtonian fluid flow around a confined cylinder in a rectangular duct, for Reynolds numbers below 40 and aspect ratios (*AR*) between 1 and 8. The experiments rely on flow visualizations, using streakline photography, and detailed velocity measurements by Particle Image Velocimetry (PIV). The experiments show unexpected velocity peaks near the side walls downstream of the cylinder even for very high aspect ratios. Increasing inertia enhances this unexpected three-dimensional phenomenon. The experimental results show that recirculations appear downstream of the cylinder for Reynolds number around 6. The comparison of the experimental results with the corresponding predictions shows good agreement.

***Keywords:*** *Confined cylinder flow; three-dimensional effects; velocity peaks.*

## 1 Introduction

Flows around a confined circular cylinder of Newtonian and non-Newtonian fluids, especially those exhibiting viscoelasticty, are of relevance in a variety of industrial applications, hence they deserve to be studied in detail. As typical examples, these flows are intrinsically related with important applications in heat exchangers, food processes, in flow through porous media or in textile coating processes [1]. Their practical implementation leads to three-dimensional flow exhibiting features not present in traditional studies using two-dimensional geometries [2], which is one of the established benchmarks in the development of numerical methods for non-Newtonian fluids [3]. The study of three-dimensional effects in laminar flow around a confined cylinder is relatively recent and other studies on 3D effects are often numerical [4, 5]. The numerical investigation of the flow in a backward facing step preceded by a smooth contraction of Poole et al [4] has shown the appearance of velocity peaks near the neutral side walls but these effects are due to the non-newtonian behaviour of the fluids used. Ferreira [5] studied numerically the three-dimensional flow effects around confined cylinders for both Newtonian and non-Newtonian fluids and also found the appearance of peak velocity near the side walls. It is not yet clearly established when the flow can be considered two-dimensional, and what are the flow characteristics when the flow is three dimensional.

This work aims to help clarify some of the issues on three-dimensional effects via an experimental and numerical investigation programme for Newtonian fluids flowing across a cylinder confined in a channel with a a blockage ratio of 50% (ratio between the cylinder diameter and the depth of rectangular section) and at Reynolds numbers below 40, that is approximately the critical value for the onset of vortex shedding [6]. In the future this study will be extended for non-Newtonian fluids. The effect of the aspect ratio, *AR* (ratio between the width of the rectangular section and its depth) will also be analyzed in detail using the numerical simulations and after validation against a set of experimental data for $AR = 8$. The working fluids were water and an aqueous solution of glycerine (46.3 wt %).

The experimental set-up and measurement techniques are described in section 2. Experimental and numerical results are discussed and compared in section 3. Section 4 presents the conclusions of this work.

# 2 Experimental System

## 2.1 Experimental Set-up

A schematic overview of the experimental set-up is shown in Figure 1 a). The test section is a 1.7 m long rectangular duct (column - CL) with a depth ($H$) of 20 mm and a variable width ($L$), where the confined cylinder is located. The variable width allows the variation of aspect ratio between 1 and 8, but the experiments in this study are restricted to $AR$ = 8 (Figure 1 b)). The cylinder is located 0.63 m downstream of the duct inlet and is positioned at the mid plane to define a symmetric geometry with a 50% blockage *(D/H)*.

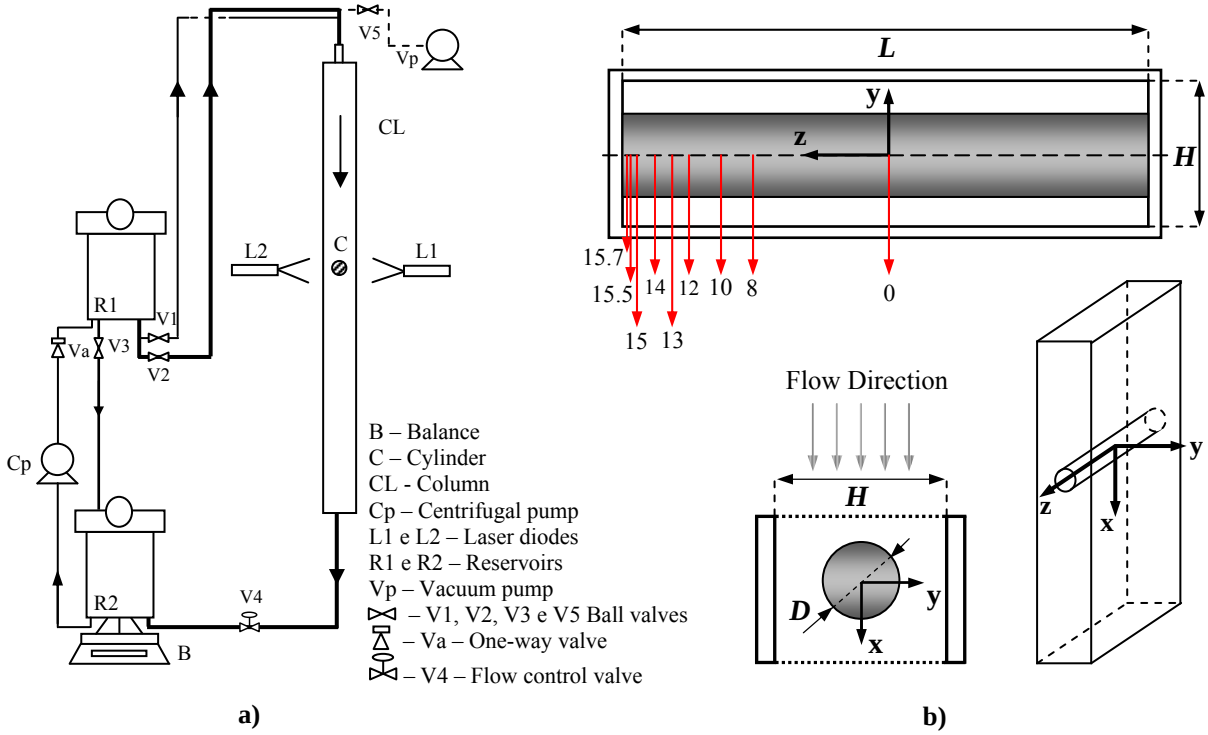


**Fig.1.** a) Test section; b) coordinate system.

The fluid flows through the column by gravity (from reservoir R1 to reservoir R2) and a centrifugal pump (Cp) forces the fluid back to reservoir R1. This pump is switched off for a few seconds when the flow rate is measured, using a scale that is placed under reservoir R2.
All the experiments were carried out at Reynolds numbers (based on cylinder radius) between 7 and 40, in order to maintain steady flow, as concluded by Ferreira [5]. In addition, in all experiments the flow was symmetric with respect to planes $y = 0$ and $z = 0$ as will be confirmed from the experimental and numerical results. The fluids used were water and an aqueous solution of glycerine (46.3 wt %) with 20 ppm of PVC tracer particles (diameter of 50 μm) used to visualize the flow patterns and in the Particle Image Velocimetry (PIV) measurements.

## 2.2 Measurement Techniques

The experiments rely on flow visualizations, using streak line photography, and detailed velocity measurements by Particle Image Velocimetry (PIV), both taken in various $z$ planes that cross the cylinder. Figure 1 b) shows the planes under study: $z/R$ = 0, 8, 10, 12, 13, 14, 15, 15.5 and 15.7.
The flow visualizations used two 5 mW laser diodes (L1 e L2) equipped with cylindrical lens to create a light sheet perpendicular to the axis of the cylinder, to illuminate the tracer particles in suspension. The two laser diodes are used to minimize the shadows around the cylinder. The pictures were taken with a digital camera (CANON EOS 30D with a macro EF100mm f2.8 lens) and the exposure time used varied from 1s to 30s, depending on flow velocity.
The detailed measurements of velocity fields were carried out using a PIV system from Dantec. The fluid was illuminated by a double pulsed laser light (Solo PIV III of New Wave Research), which generates consecutive

pairs of light sheets with a wavelength of 532 nm and a maximum energy of 50 mJ per pulse. The two consecutive pulses of light illuminated the suspended particles which refracted light containing the information that allowed the determination of the corresponding velocities from the displacement of the imaged particles. These images were acquired using a digital CCD camera (Flow Sense 2M, Dantec Dynamics), with a Nikon AF Micro lens of 60 mm focal length. A total of 50 image pairs were acquired in each experiment and post-processed using FlowManager v4.60 software from Dantec Dynamics. The adaptive correlation was used on interrogation windows ranging between 32 by 32 pixels to 16 by 16 pixels, depending on the plane under study [7].

### 2.3 Numerical procedure

For the numerical calculations, an in-house finite-volume numerical method was used. This finite-volume code and its procedures have been extensively used and validated [1]. Numerical calculations are used to compare with experimental results and to investigate flow conditions not measured.

## 3 Results and Discussion

Figures 2 and 3 show two sets of streakline photographs obtained during the flow visualizations to illustrate the variation of recirculation length, $L_V$, with the spanwise coordinate at a fixed Reynolds number (Fig. 2) and the increase in recirculation length with Reynolds number at a fixed location (Fig. 3). Many more photographs were taken to allow construction of Figure 4 which shows the spanwise variation of the recirculation length at several Reynolds numbers in the range $7.2 \leq Re \leq 40$ and compares the measured profiles with the corresponding calculated profiles. At all spanwise locations the recirculation length increases with Reynolds number, but shows the existence of three peak values. There is a maximum recirculation at the side wall, followed by an intense reduction in $L_v$ at about $z/R = \pm 15$ followed by an increase to a plateau value, except at the higher Reynolds numbers where $L_v$ reaches a maximum value at about $z/R = \pm 10$, before levelling to the plateau value. Therefore, the recirculation length is minimum at the plane $z/R = \pm 15$ and maximum in the core or at $z/R = \pm 10$ for $Re \geq 27.3$ as shown in Figure 4. The comparison between the experimental and numerical results is excellent and the numerical calculations confirming the flow symmetry and following all the details observed experimentally.
It is not so clear in the experiments, but at low Reynolds number the recirculation length is actually maximum at the side walls, whereas at large Reynolds numbers the recirculation length at the side wall is shorter than elsewhere except at $z/R = \pm 15$. This will be further discussed later, when analysing in more detail the result of numerical calculations.

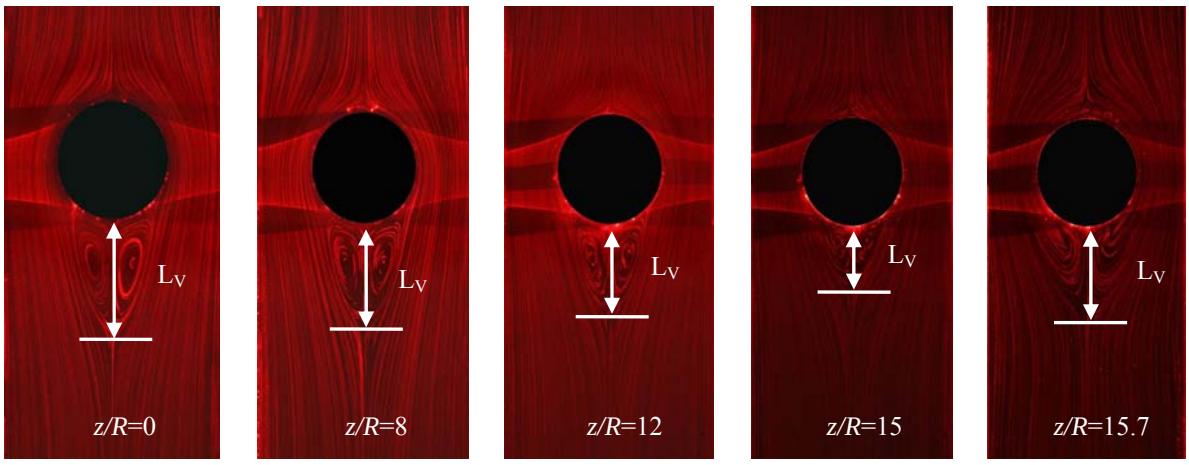


**Fig. 2.** Streakline photographs at Re = 20.0 for some planes under study.

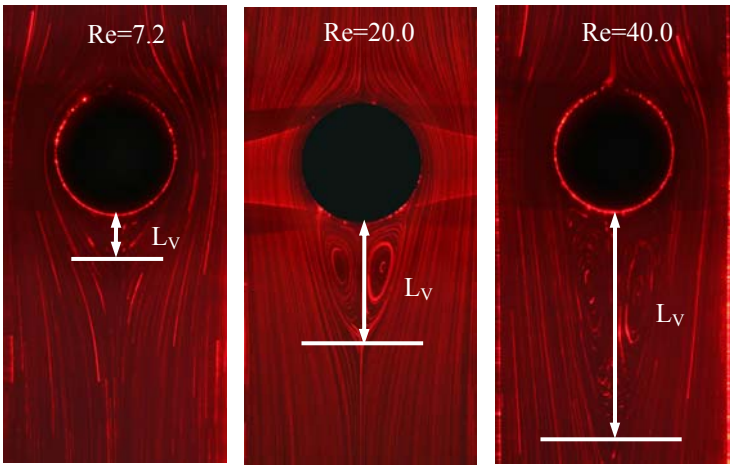


**Fig. 3.** Streakline photographs at $z/R = 0$ for Re = 7.2, 20.0 and 40.0.

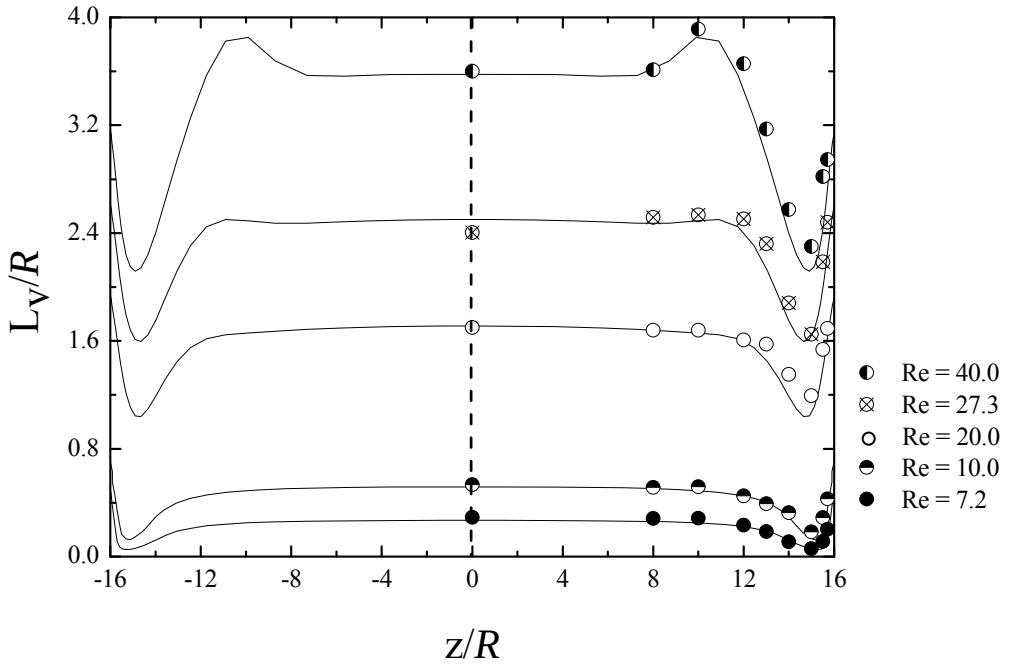


**Fig.4.** Recirculation length for several Reynolds numbers for each plane under study (symbols) and comparison with numerical predictions (curves).

Figure 5 a) shows profiles of normalized streamwise velocity along the centerline (normalized coordinates ($x/R$, 0, 0)) at different Reynolds numbers, Re = 17.3 and Re = 26.6, whereas figure 5 b) compares profiles of normalized streamwise velocity along the centerlines (coordinates ($x/R$, 0, $z/R$)) at different spanwise planes, $z/R$ = 0 and $z/R$ = 15 for Re = 17.3. These profiles were measured by PIV and as is clear from figure 5 a), upstream of the cylinder the two profiles tend to coincide and the flow is only affected by the presence of the cylinder within a distance of 4 radii of the cylinder center. Downstream of the cylinder, one can clearly observe the existence of the recirculation and the increase of its length with the increase of Reynolds number, in agreement with the flow visualization results. In Figure 5 b) the fluid velocity upstream of the cylinder is greater on the centre plane ($z/R = 0$) than near the side wall ($z/R = 15$) as is expected from the fully developed profile in this rectangular channel. In this respect note that the Reynolds number of the duct flow based on the channel width is twice the cylinder flow Reynolds number and for $Re_{duct} \approx 35$ the length needed for flow development is of the order of one tenth of the distance between the duct inlet and the cylinder. Also in Figure 5 b), downstream of the cylinder one can observe that in the plane near the side walls ($z/R = \pm 15$), where the recirculation length is

minimum, the fluid velocity is maximum, i.e. the flow has reattached earlier and the velocity developed quicker in spite of the retarding presence of the side walls. Further downstream, however, the retarding effect of the side wall makes itself noticeable, as the velocities at $z/R = 0$ exceed the near side wall velocities. Figures 5 a) and 5 b) include also as lines the results of the corresponding numerical calculations and again the comparison between experimental and numerical results is good.

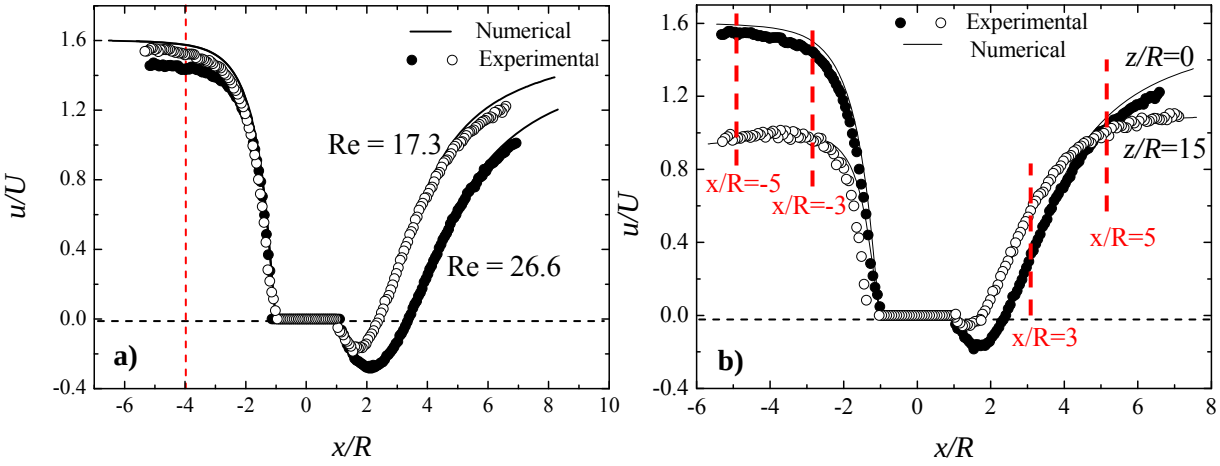


**Fig. 5.** Velocity profiles along the centerline ($y/R = 0$): a) at $z/R = 0$ for Re = 17.3 and Re = 26.6; b) at Re = 17.3 for $z/R = 0$ e $z/R = 15$.

Figures 6 a) to 6 d) show transverse profiles of the axial velocity for Re = 17.3 along the $y$-axis at $x/R$ = -5, -3, 3 and 5, respectively, at the planes $z/R = 0$ and $z/R = 15$. These streamwise locations ($x/R$) are also marked in Figure 5 b). Only half of the profiles are represented, since there is symmetry of the velocity profiles. Upstream of the cylinder, Figure 6 a) shows the approach of a fully-developed profile. This profile is not influenced by the presence of the cylinder, which at this Reynolds number is limited to about 4 cylinder radii as discussed previously in respect to Figure 5 a).

In Figure 6 b), the profile is closer to the cylinder ($x/R$ = -3) and one can already observe a flow deceleration in the center, by comparison with Figure 6 a). In contrast, near the side wall there is flow acceleration, even though the effect is quite small, suggesting the appearance of a small spanwise velocity component towards the side wall concomitant. This axial velocity decrease is due to the blockage by the cylinder and becomes more pronounced as the cylinder is approached.

Downstream of the cylinder at $x/R = 3$ (Figure 6 c)) the velocities are higher near the side walls ($z/R = \pm 15$) than at the centre plane ($z/R = 0$) for $|y/R| < 0.6$ on account of the earlier flow recovery (shorter recirculation). These higher velocities confirm the existence of velocity peaks in the $y$ direction, which are strongly enhanced by increasing flow inertia and the location of which also depend on Reynolds number. For $|y/R| > 0.6$ the axial velocities are larger in the core than near the side walls, because in the approach flow the local flow rate is also higher in the center than near the side walls, i.e., the appearance of a spanwise velocity component does not change significantly the distribution of flow rate along the $z$ direction.

In Figure 6 d), pertaining to $x/R = 5$, the velocity in the centre plane ($z/R = 0$) is nearly equal of velocity near the side walls ($z/R = \pm 15$) at $y/R = 0$. Inspection of Figure 5 b) shows that this plane is at the cross-over point of the axial profiles of axial velocity at the centreplane, at this particular Reynolds number. As we are now further downstream of the cylinder than in Figure 6 c), the velocity peaks in the jet between cylinder and transverse wall are now obviously smaller than at $x/R = 3$.

In all cases, and as shown in Figures 4 - 6, the comparison between experimental and numerical results is quite good and validates the numerical calculations. Hence, numerical calculations can be carried out to quickly investigate in detail other flow conditions not measured experimentally.

Figure 7 shows the numerical results of the recirculation length as a function of Reynolds number at different aspect ratios, in order to study the combined influences of aspect ratio and Reynolds number on the flow behaviour. Figures 7 a) and 7 b) pertain to $AR = 2$ and $AR = 1$, respectively, and show profiles of the recirculation length at the same Reynolds numbers of 10, 20 and 40 that were reported in figure 3 for $AR = 8$.

Figure 7 a) shows the appearance of velocity peaks near the side walls for lower Reynolds numbers. At $AR = 2$, for higher Reynolds number (Fig. 7 a)) and $AR = 1$ (Fig. 7 b)) the effect of Reynolds number shown is globally similar to that seen at $AR = 8$ (Fig 4). The main differences are apparent in the comparison between the two plots, especially at large Reynolds numbers. The profiles of $L_v$ at low Reynolds number have similarities with a

maximum length at the wall followed by a minimum value and an increase towards the center. The reduction of aspect ratio smears the valley where $L_v$ becomes a local minimum and widens the region of maximum $L_v$, but this is also a consequence of the normalization. At large Reynolds numbers, however, $L_v$ is a local maximum at the side walls for $AR = 1$, but only a local maximum at $AR = 8$. The global minimum near the wall is present in both cases, but whereas for $AR = 8$ this maximum is next to the local minimum, and so we find a local maximum on each side of the profile, for smaller $AR$ they have merged into a single maximum at the $z/R = 0$ center plane.

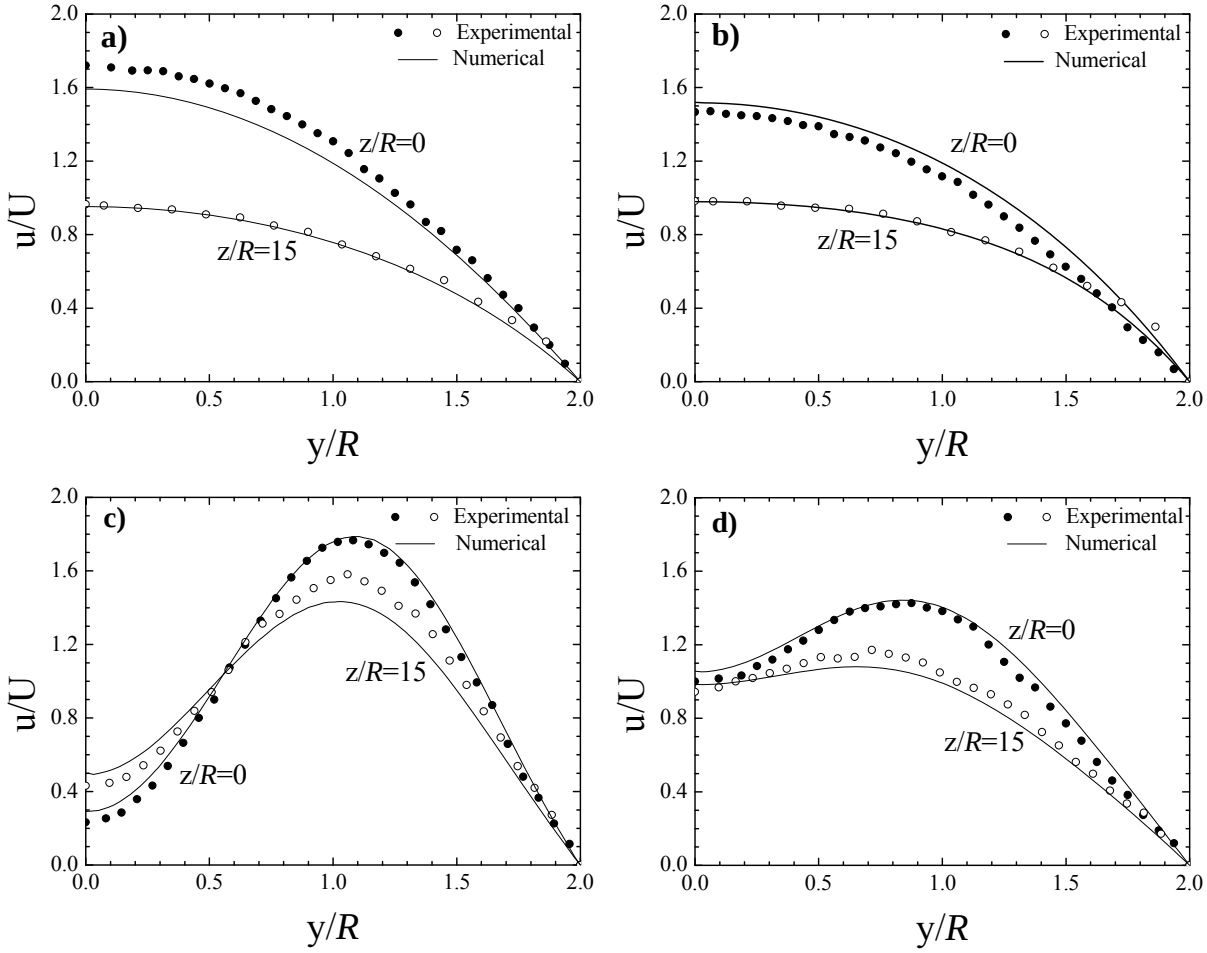


**Fig. 6.** Effect of spanwise coordinate $y$ on transverse profiles of axial velocity for $Re = 17.3$ at: a) $x/R = -5$, b) $x/R = -3$, c) $x/R = 3$ and d) $x/R = 5$.

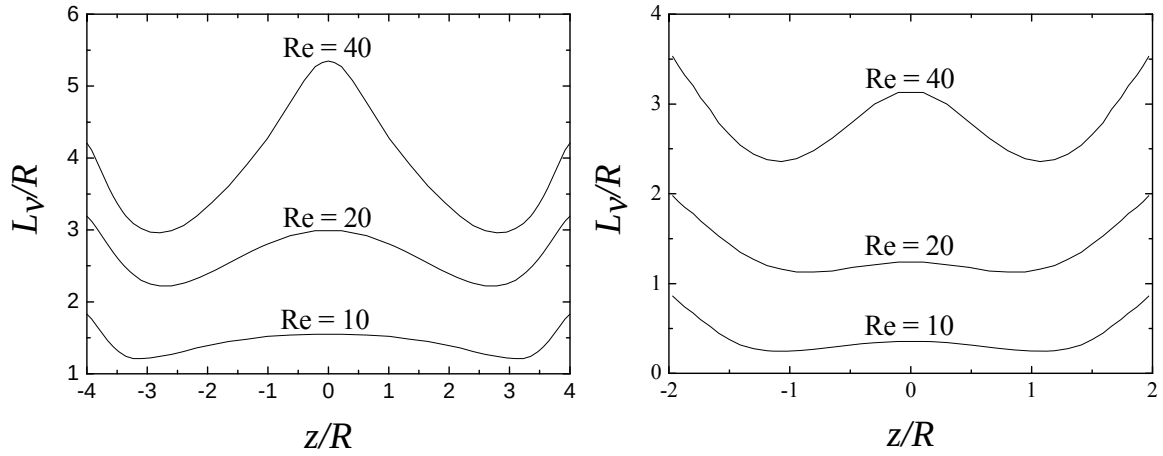


**Fig. 7.** Variation of recirculation length as a function of Reynolds number at y/R=0: a) $AR = 2$; b) $AR = 1$.

Profiles of streamwise velocity downstream of the cylinder at $y/R = 0$, shown in Figures 8 a) and b) for $AR = 8$ and 1, respectively, have an inverse shape to the corresponding profiles of $L_v$, i.e., where there is a local maximum in $L_v$ we find a local velocity minimum and vice versa.
So, the results show the existence of velocity peaks near the side walls, which are enhanced by flow inertia, but the difference in the behaviour at $AR = 8$ and $AR = 1$, even at high Reynolds number, is a consequence of the qualitative differences in the two flows which come from the different effect the side walls exert on the flow at the core of the duct. In effect, the comparison between the velocity profiles of Figure 8 a) and 8 b) show a major distinction. The profiles at the lower Reynolds number ($Re = 10$) develop fast and whereas for $AR = 8$ the value of $u/U$ at the centre plane is about 1.5, typical of a channel flow, for $AR = 1$ one gets $u/U \approx 2$ at the centre, which is typical of a flow in a pipe or in a geometry where the action of viscous stresses come from all sides. Hence, whereas for $AR = 8$ the influence of the side wall is confined to a region near the side walls and does not come to the centre of the duct where the flow is essentially controlled by the vicinity of the other two walls, for $AR = 1$ the side walls are as important as the other two walls and affect the flow at the centre plane. This will naturally affect the size and strength of the side walls velocity peaks, which predictably will be similar to those seen for $AR = 8$ for, say, $AR \geq 4$, whereas the picture will change dramatically as $AR$ is reduced to zero, to the Hele-Shaw flow limit.

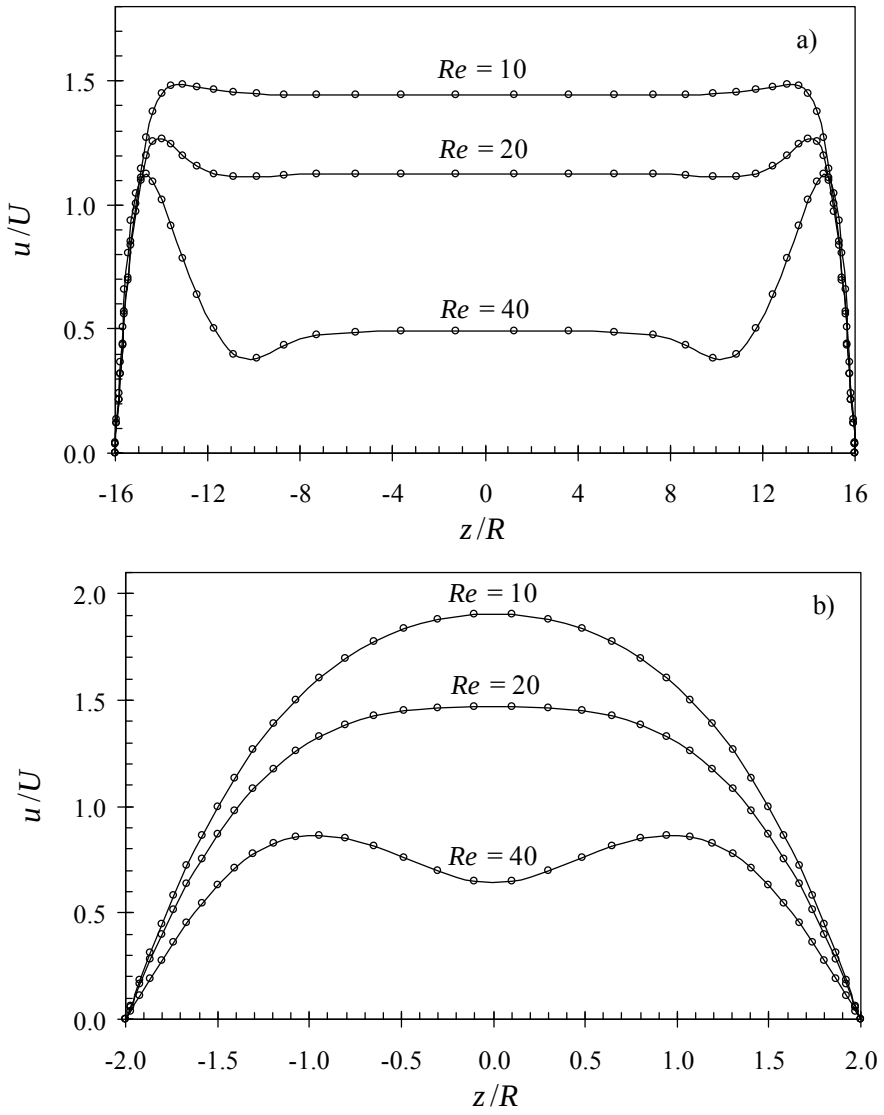


**Fig. 8.** Profiles of axial velocity at $y/R = 0$ and $x/R = 6$ as a function of spanwise coordinate ($z/R$) for various Reynolds number at: a) $AR = 8$; b) $AR = 1$.

## 4. Conclusions

An experimental and numerical investigation was carried out on the Newtonian flow around a confined cylinder placed in a rectangular duct with a 50% blockage ratio. The Reynolds varied between 7 and 40 and the aspect ratio varied between 1 and 8.
The experiments relied on flow visualizations, using streakline photography, and detailed velocity measurements by Particle Image Velocimetry, both taken in various planes around the cylinder. The numerical calculations were carried out with a finite volume numerical method and compared very well with experimental results. The good agreement between numerical and experimental results indicated that a further study could be carried out numerically to explore flow conditions not studied experimentally and to help to interpret the results.
The results obtained in the detailed velocity measurements for the $AR = 8$ case show that the upstream influence of the cylinder is restricted to within 4 radii of the cylinder center. Downstream of the cylinder, there were two velocity peaks near the side walls ($z/R = \pm 15$). These peaks are probably due to the incapacity of the low velocity fluid to negotiate the adverse pressure gradient downstream of the cylinder in regions just outside the side wall. Inertia was found to increase the recirculation length regardless of the aspect ratio of the duct. For large $AR$, the observed velocity peaks near the side walls corresponded to locations where the recirculation was a local minimum. These features were also present at $AR = 1$ and 2, even though with lower intensity on account of the smearing effect of viscosity.
Next to the side walls velocity peaks, there were small velocity troughs corresponding to slightly longer recirculations especially at the higher Reynolds numbers. For the $AR = 1$ geometry these two velocity troughs had merged into a single one localized at the centreplane and corresponding to a local maximum recirculation length.

## Acknowledgements

The authors gratefully acknowledge funding by Fundação para a Ciência e Tecnologia (FCT) and FEDER via projects REEQ/262/EME/2005, REEQ/928/ EME/2005, PTDC/EQU-FTT/71800/2006 and PTDC/EME-MFE/70186/2006. VMR also acknowledges financial support of FCT through scholarship SFRH/BD/44737/2008.

## References

1. M.A. Alves, F.T. Pinho and P.J. Oliveira, The flow of viscoelastic fluids past a cylinder: finite-volume high-resolution methods*, J. Non-Newt. Fluid Mech*., 97, 207-232, 2001.
2. J.M. Verhelst and F.T.M. Niewstadt, Visco-elastic flow past circular cylinders mounted in a channel: experimental measurements of velocity and drag, *J. Non-Newt. Fluid Mech*., 116, 301-328, 2004.
3. R. A. Brown and G. H. McKinley, Report on the VIIIth International Workshop on Numerical Methods in Viscoelastic Flows. Journal of Non-Newtonian Fluid Mechanics, 52, 407-413
4. R.J. Poole, M.P. Escudier, A. Afonso and F.T. Pinho, Laminar flow of a viscoelastic shear-thinning liquid over a backward-facing step preceded by a gradual contraction, *Phys. Fluids*, 19, 93-101, 2007.
5. H.H. Ferreira, Escoamento de fluidos newtonianos e viscoelásticos em torno de um cilindro: Estudo numérico de efeitos tridimensionais, MSc Thesis, FEUP, 2007.
6. M. Sahin and R.G. Owens, A numerical investigation of wall effects up to high blockage ratios on two-dimensional flow past a confined circular cylinder, *Physics of fluids,* volume 16, number 5 2004.
7. V.M. Ribeiro, H.E. Ferreira, P.C. Sousa, P.M. Coelho, F.T. Pinho and M.M. Alves, Three-dimensional effects in low Reynolds number flow around confined cylinders, Paper 2.2.3. Pdf in Proceedings of 14th Int. Symp. On Applications of Laser Techniques to Fluid Mechanics, Lisbon, Portugal, 07-10 July 2008.